Available online at www.sciencedirect.com
ScienceDirect
Carbohydrate Research 342 (2007) 2086–2096
Carbohydrate RESEARCH

New Karplus equations for $^{2}J_{HH}$, $^{3}J_{HH}$, $^{2}J_{CH}$, $^{3}J_{CH}$, $^{3}J_{COCH}$, $^{3}J_{CSCH}$, and $^{3}J_{CCCH}$ in some aldohexopyranoside derivatives as determined using NMR spectroscopy and density functional theory calculations

Mohsen Tafazzoli* and Mina Ghiasi

Department of Chemistry, Sharif University of Technology, PO Box 11365-9516 Tehran, Iran

Received 20 January 2007; received in revised form 17 April 2007; accepted 20 May 2007
Available online 2 June 2007

Abstract—The ^{1}H–^{13}C coupling constants of methyl α- and β-pyranosides of D-glucose and D-galactose have been measured by one-dimensional and two-dimensional ^{1}H–^{13}C heteronuclear zero and double quantum, phase sensitive *J*-HMBC spectra to determine a complete set of coupling constants ($^{1}J_{CH}$, $^{2}J_{CH}$, $^{3}J_{CH}$, $^{2}J_{HH}$, and $^{3}J_{HH}$) within the exocyclic hydroxymethyl group (CH_2OH) for each compound. In parallel with these experimental studies, structure, energy, and potential energy surfaces of the hydroxymethyl group for these compounds were determined employing quantum mechanical calculations at the B3LYP level using the 6-311++G** basis set. Values of the vicinal coupling constants involving ^{1}H and ^{13}C in the C5–C6 (ω) and C6–O6 (θ) torsion angles in the aldohexopyranoside model compounds were calculated with water as the solvent using the PCM method. To test the relationship between $^{3}J_{CXCH}$ (X = C, O, S) and torsion angle C1–X (φ) around the anomeric center, the conformations of 24 derivatives of glucose and galactose, which represent sequences of atoms at the anomeric center of C-glycosides (C–C bond), O-glycosides (C–O bond), thioglycosides (C–S bond), glycosylamines (C–N bond), and glycosyl halides (C–halogen (F/Cl) bond) have been calculated. Nonlinear regression analysis of the coupling constants $^{1}J_{C1,H1}$, $^{2}J_{C5,H6R}$, $^{2}J_{C5,H6S}$, $^{2}J_{C6,H5}$, $^{3}J_{C4,H6R}$, $^{3}J_{C4,H6S}$, $^{2}J_{H6R,H5}$, and $^{3}J_{H5,H6R}$ as well as $^{3}J_{CXCH}$ (X = C, O, S) on the dihedral angles ω, θ, and φ have yielded new Karplus equations. Good agreement between calculated and experimentally measured coupling constants revealed that the DFT method was able to accurately predict *J*-couplings in aqueous solutions.

Keywords: Karplus; Glucose; Galactose; NMR; *J*-HMBC; DFT

1. Introduction

Carbohydrates are an important class of biomolecules that are commonly found in nature in different forms such as monosaccharides, oligosaccharides, and polysaccharides. They contain several conformational domains such as the exocyclic hydroxymethyl (CH_2OH) fragment of monosaccharides and glycosidic linkages of oligo- and polysaccharides. The conformation about the exocyclic C5–C6 bond is important in the determination of the three-dimensional structures of carbohydrate molecules. Although the conformational properties around the C5–C6 bond have been the subject of several investigations including both experimental and theoretical studies,[1–3] the factors that control the conformational behavior of the exocyclic C5–C6 linkage are still not perfectly understood. In addition, one of the key objectives of conformational studies of oligosaccharides in solution is the estimation of the torsional behavior of their component glycosidic linkages involving a heteroatom that is designated as $^{3}J_{CXCH}$ (Scheme 1). The glycosidic torsion angles φ and ψ are usually determined from NOE measurements between protons near to the linkage (H1 and H3′, Scheme 1).[4] Generally the number of observable NOEs sensitive to φ and ψ, especially in

* Corresponding author. Tel.: +98 21 66005718; fax: +98 21 66012983; e-mail: Tafazzoli@sharif.edu

0008-6215/$ - see front matter © 2007 Elsevier Ltd. All rights reserved.
doi:10.1016/j.carres.2007.05.032

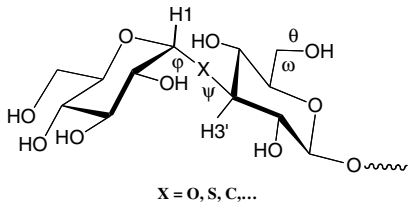

Scheme 1. Conformational domains of oligosaccharides.

smaller structures, is limited and thus linkage conformation is often difficult to assess in this manner.[5] Thus, studies of *J*-coupling would benefit greatly from reliable computational tools that permit their accurate calculations in the actual molecules under investigation, or in a closely related structure. These theoretical methods could also be applied to test predictions made via experiments and provide new complementary data to derive more stable structure *J*-coupling correlations.

In the present work, we are interested in extending the use of *J*-coupling constants for structural, stereochemical and conformational analysis of carbohydrates, by determining the dependencies of $^{3}J_{HH}$, $^{2}J_{HH}$, $^{2}J_{CH}$ and $^{3}J_{CH}$ coupling constants on the ^{1}H–^{13}C atomic dihedral angles in some aldohexopyranoside derivatives. Thus, 24 derivatives of glucose and galactose (Scheme 2), which have both anomeric configurations of the C–O bond in glycosides (**1a**–**d**), the C–S bond in thioglycosides (**2a**–**d**), the C–C bond in C-glycosides (**3a**–**d**), the C–N bond in glycosylamines (**4a**–**d**), and the C–X bond in glycosyl halides (**5a**–**d**, **6a**–**d**) forms have been studied. Also, we have explored the effect of the neighboring hydroxyl group at C4 on the conformational properties of the C5–C6 linkage by using quantum mechanical methods in aqueous solution. We calculated $^{3}J_{HH}$, $^{2}J_{HH}$, $^{2}J_{CH}$, and $^{1}J_{CH}$ for the exocyclic CH_2OH group and the $^{3}J_{CXCH}$ for the X-glycosidic linkage, as a function of ω, θ and glycosidic torsion angle φ.

2. Methods

2.1. NMR measurements

^{1}H NMR, ^{13}C NMR, $^{13}C\{^{1}H\}$, COSY, HMQC, and phase sensitive *J*-HMBC spectra of methyl α- and β-pyranosides of D-glucose and D-galactose were obtained at 298 K in D_2O (99.99% D) on a Bruker DRX500 instrument operating at 500.133 MHz for ^{1}H and 125.770 MHz for ^{13}C, using a 5 mm broadband inverse probe with sufficient digital resolution to ensure errors $\leqslant$0.1 Hz in the measured *J*-couplings. Sodium 4,4-dimethyl-4-silia-[$^{2}H_4$] pentanoate was used as internal standard.

^{1}H NMR with 90° pulse (10.3 μs) and ^{13}C NMR spectra were acquired using a spectral width of 3255 Hz and 22,123 Hz, respectively. Values of $^{1}J_{C,H}$ were measured either from 1D ^{13}C NMR spectra. All 2D NMR spectra were acquired by pulsed field gradient-selected methods.

2D-correlation spectroscopy (COSY) was used to confirm ^{1}H assignments. Heteronuclear multiple quantum correlation (HMQC) and heteronuclear multiple bond correlation (HMBC) were used for ^{13}C assignments. Figure 1 shows the HMQC spectrum of methyl β-D-glucopyranoside; ^{1}H NMR δ (ppm): 4.25 (d, H1), 3.81 (dd, H6*R*), 3.62 (dd, H6*S*), 3.45 (s, CH_3), 3.38 (t, H3), 3.33 (m, H5), 3.26 (t, H4), 3.15 (t, H2); ^{13}C NMR δ (ppm): 103.6 (C1), 76.7 (C3), 76.2 (C5), 73.1 (C2), 70 (C4), 61.1 (C6), 57.7 (CH_3). HMQC, HMBC, and *J*-HMBC spectra were recorded using 2048 × 1024 data matrices and, in all cases, the number of scan and dummy scans were 48 and 16, respectively. The spectral width in COSY experiments with a pre-saturation during relaxation delay was 3255 Hz in both dimensions with 2 s relaxation delay. The HMQC, HMBC, and *J*-HMBC spectra were recorded with 2 s inter pulse delay. The spectral widths were $sw_1 \times sw_2 = 3255 \times 22{,}123$ Hz

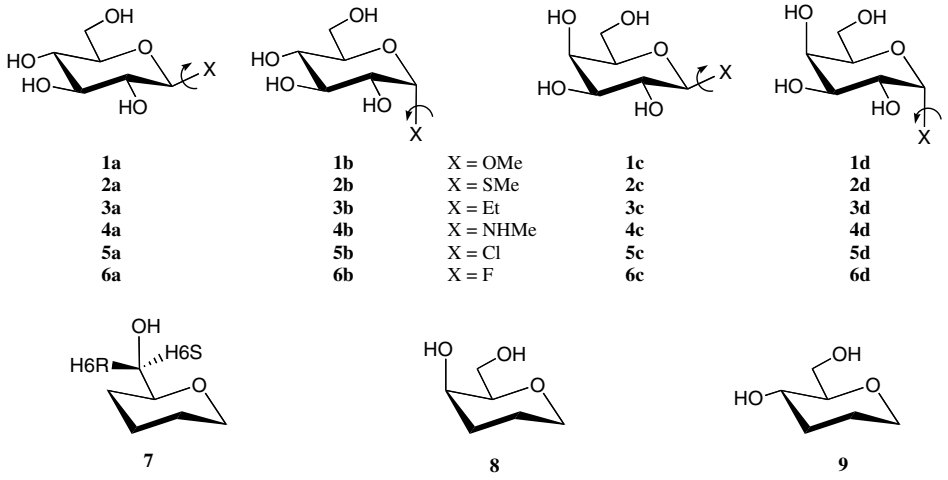

Scheme 2. Schematic representation of different derivatives of α- and β-pyranosides of D-glucose and D-galactose.

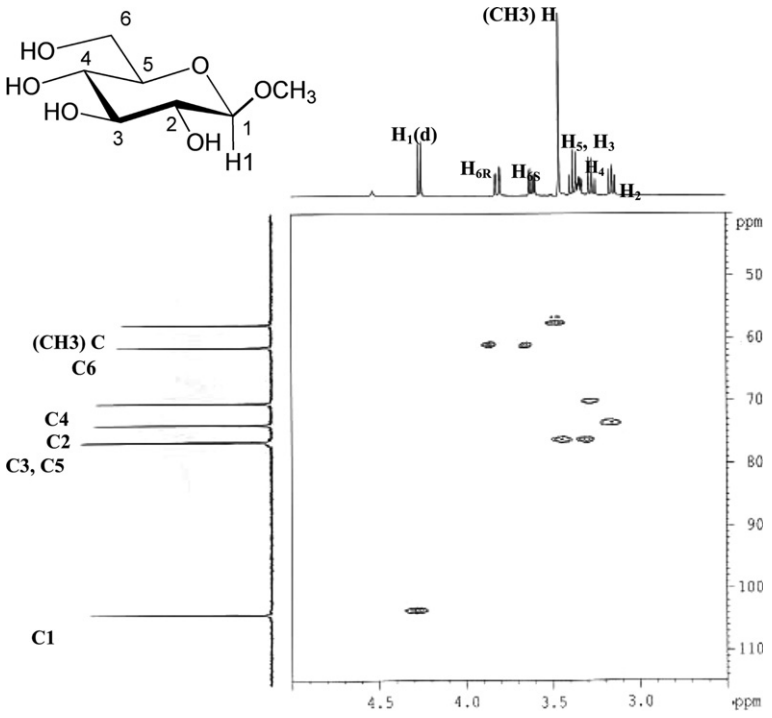

Figure 1. HMQC spectrum of methyl β-D-glucopyranoside.

in all 2D experiments. For Z gradients, the G1:G2:G3 = 50:30:40.1 gradient ratios were used for both HMQC and HMBC spectra. The phase sensitive *J*-HMBC using Echo/Anti-echo gradient selection with twofold low-pass *J*-filter to suppress one-bond correlations procedure was used in the data acquisition for obtaining pure-absorptive peak patterns.[6] To determine long range CH coupling constants, the gradient ratio G1:G3:G4:G5 = 80:15:−10:−5 was used.

2.2. Ab initio molecular orbital calculations

Ab initio calculations were carried out with GAUSSIAN 2003.[7] Geometry optimization was performed by employing a hybrid Hartree-Fock-density functional scheme, the adiabatic connection method Becke three-parameter with Lee-Yang-Parr (B3LYP) functional[8] of density functional theory (DFT),[9] with the standard 6-311++G** basis set. Full optimizations were performed without any symmetry constraints. This level of theory has been shown to give reasonable potential energy surfaces for D-aldo- and D-ketohexoses and reduces the basis superposition error that is relevant to systems with hydrogen bonds.[10] We computed the harmonic vibrational frequencies to confirm that an optimized geometry correctly corresponded to a local minimum. The solvent effects on the conformational equilibrium were investigated with the PCM method at the B3LYP/6-311++G** level. Solvation calculations were carried out for water ($\varepsilon = 78.39$) with the geometry optimization for this solvent. Conformational energy profiles around the C5–C6 bond in **1a**–**d** were calculated by driving the ω dihedral angle from 0° to 330° in 30° increments while allowing the remaining geometrical parameters relax. To estimate the effect of intramolecular hydrogen bonding, we calculated the energy profiles by fixing the corresponding protons of the hydroxyl groups at C6 and C4 in the *ap* conformation, so that hydrogen bonds between these groups were excluded. In this report, the orientations about the C5–C6, C6–O6, and C1–X bonds are described by torsion angles (ω = O5–C5–C6–O6), (θ = C5–C6–O6–H), and (φ = H1–C1–X–C), where X is O (in **1a**, **b**, **c**, **d**), S (in **2a**, **b**, **c**, **d**), C (in **3a**, **b**, **c**, **d**), N (in **4a**, **b**, **c**, **d**), Cl (in **5a**, **b**, **c**, **d**) or F (in **6a**, **b**, **c**, **d**). For the C5–C6 rotamers, we used the standard nomenclature (Scheme 3); O5 and C4 are the reference atoms and staggered conformers are designated as *gt* ($\omega \approx 60$), *tg* ($\omega \approx 180$) or *gg* ($\omega \approx -60$).

2.3. Calculation of NMR spin–spin coupling constants

Recent investigations have shown that density functional theory (DFT) can be used to calculate reliable J_{CH} and J_{CC} values in carbohydrates without scaling.[11,12] DFT-computed J_{CH} and J_{CC} values were estimated to be within 5% and 10%, of experimental values, respectively. In the present work, we extend this approach to calculate *J*-coupling constants using the DFT method.

^{1}H and ^{13}C NMR spin–spin coupling constants in the DFT-optimized structure in the presence of solvent were obtained by finite-field (Fermi-contact) double perturba-

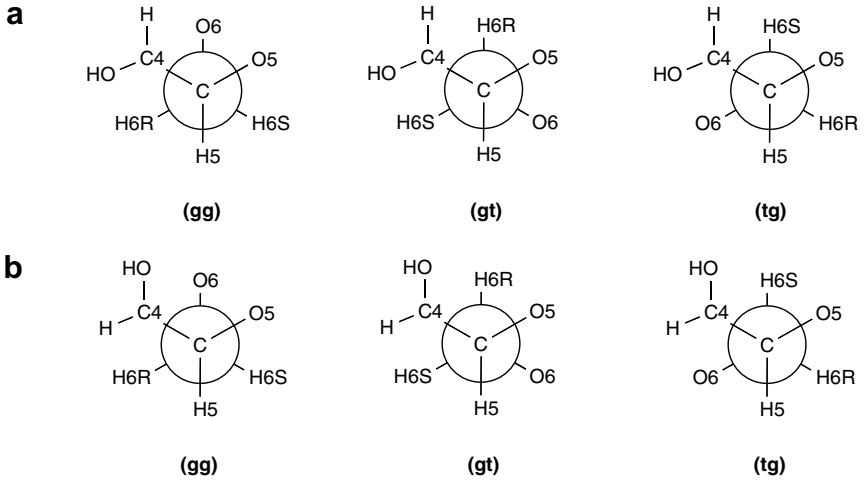

Scheme 3. Schematic representation of the *gg*, *gt*, and *tg* conformers around the C5–C6 bond showing the labeling of atoms for the (a) equatorial and (b) axial orientation of the C4 hydroxyl group.

tion theory[13] calculations at the B3LYP level using an extended basis set ([5S2P1d/3S1d]) previously designed for similar systems.[14] Appropriate values for the perturbing fields imposed on the coupled nuclei were chosen to ensure sufficient numerical precision while still allowing a satisfactory low-order finite-difference representation of the effect of the perturbation. Only the Fermi-contact component of each coupling constant was considered due to the dominant relationship of this term in J values involving carbon and hydrogen, especially in saturated systems. All the equations describing the dependencies of $^1J_{CH}$, $^2J_{CH}$, $^3J_{CH}$, and $^3J_{HH}$ on ω, θ, and φ were parameterized from the calculated couplings using a least-squares procedure.

The model compound **7** (Scheme 2) was used in the calculation of coupling constants, which are sensitive to ω and θ angles. In this model, complications caused by the arbitrary introduction of intramolecular hydrogen bonds during the geometric optimizations were reduced by the lack of a hydroxyl group at C4. The ω and θ torsion angles in compound **7** were varied systematically from 0° to 360° in 30° increments by holding both torsion angles at fixed values in the calculations. All other molecular parameters were geometrically optimized.

A second series of coupling constant calculations were performed on compounds **8** and **9** (Scheme 2), which contain an equatorial or axial hydroxyl substituent at the C4 position. In each calculation, one set of C–O torsion angles, C_5–C_4–O_4–OH_4 was fixed and only the three staggered rotamers about ω were studied. These calculations were performed to clarify the effect of OH on J-couplings involving C4 or H4. These calculations restricted rotation to a limited number of C–O torsion angles to avoid intramolecular H-bonding between O4 and O6 and their attached protons.

A third series of calculations were performed on **1a**, **2a**, and **3a** to explore the torsional dependence of $^3J_{CXCH}$ for dihedral angles φ in the range of 60–150°. All structures were fully geometrically optimized in H_2O solvent.

3. Results and discussion

3.1. Geometries optimization and energies of 1a–6d

All structures were fully optimized at B3LYP method using the 6-311++G** basis set with no initial symmetry restrictions and assuming the C_1 point group. For **1a** structure, the initial C1–O1 torsion angle, φ (Scheme 2), was chosen to optimize the *exo*-anomeric effect[15] (C2 *anti* to C, Fig. 2).

Because the complexity of the conformational equilibrium is believed to be a combination of several factors such as solvent effects,[16] we reoptimized all structures by considering the solvent effect ($\epsilon = 78.39$) using the polarized continuum (overlapping spheres) model (PCM) of Tomasi et al.[17] Table 1 summarizes the total

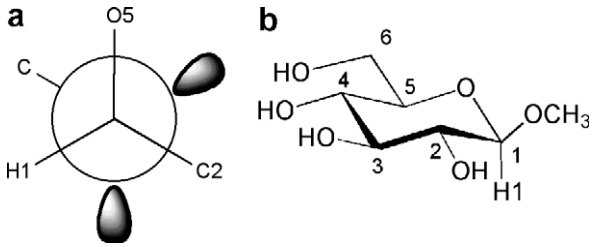

Figure 2. (a) Newman projections defining the initial values of φ. (b) Atom number scheme to facilitate comparison of labels in Newman projection.

Table 1. Free energy differences between the equatorial and axial substituents on gluco- and galactopyranosyl rings by the B3LYP/6-311++G** method in water

ΔE (kcallmol)			
E_{1a}–E_{1b}	−1.94	E_{6c}–E_{6d}	−1.55
E_{2a}–E_{2b}	−1.93	E_{6c}–E_{6d}	−1.09
E_{3a}–E_{3b}	−2.86	E_{6c}–E_{6d}	−2.74
E_{4a}–E_{4b}	−2.07	E_{6c}–E_{6d}	−0.21
E_{5a}–E_{5b}	−2.14	E_{6c}–E_{6d}	−1.58
E_{6a}–E_{6b}	−2.18	E_{6c}–E_{6d}	−1.85

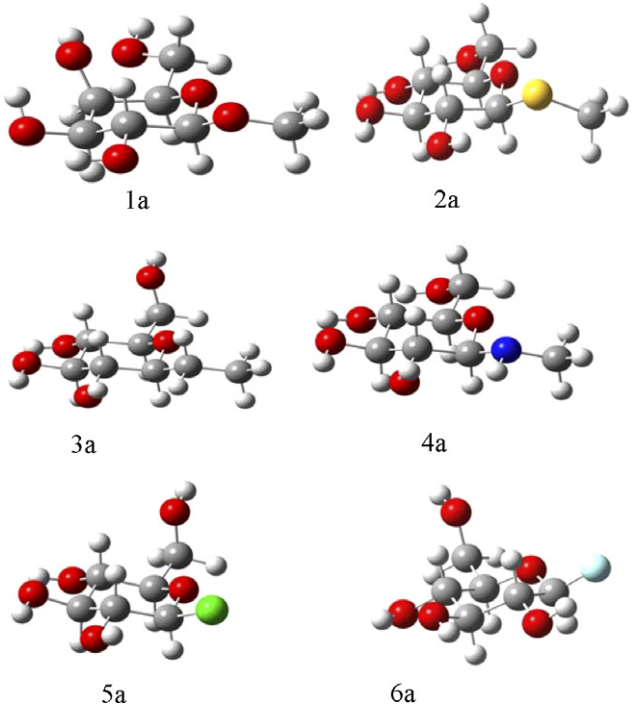

Figure 3. Three-dimensional representations of some optimized structures.

calculated electronic relative stability energies in water between the equatorial and axial substituents on the gluco- and galactopyranosyl ring. As shown in this table, for all compounds, the β-anomer is more stable than the α-anomer. Figure 3 shows some optimized structures and a selection of calculated bond distances, bond angles, and dihedral angles, which are compiled in Table 2. For all geometries, vibrational frequency calculations have confirmed stationary points with no negative eigenvalues observed in the force constant matrix.

3.2. Conformational preferences of hydroxymethyl group

To examine the effect of the C4 hydroxymethyl group on the conformation around the C5–C6 bond, we have studied methyl α- and β-pyranosides of D-glucose and D-galactose, **1a**–**d**. Conformational analysis of these compounds is a convenient way to show the effect of internal hydrogen bond effect on rotamer population.[18] The B3LYP/6-311++G** conformational energy profile for the β anomer (**1a**), considering the solvent effect for rotation around the C5–C6 bond, is presented in Figure 4. The corresponding α anomer shows a similar profile so the data are not presented. The solid line shows the calculated profiles with full optimization for a given value of the ω angle. The dashed line represents calculated profile with orientations of H(O4) and H(O6) hydrogens in the *ap* local minimum to avoid steric conflict and intramolecular hydrogen bonding. It is clear that when the hydroxyl groups are allowed to interact by hydrogen bonding (solid line), their conformational profiles differ from those without hydrogen bonds (dashed lines) and from profiles calculated for model compounds without the C4 hydroxyl group.[19,20] For **1a**, the results predict four minimum points for torsional potential energy and that the two deep minima at $\omega = 150°$ and 240° are due to

Table 2. Selected structural details of optimized structures, bond distances (Å) and bond and dihedral angles (°)

	1a	**1b**	**2a**	**2b**	**3a**	**3b**	**4a**	**4b**	**5a**	**5b**
Bond distances										
C1–C2	1.52	1.53	1.54	1.54	1.53	1.54	1.53	1.54	1.53	1.54
C2–C3	1.52	1.52	1.52	1.54	1.52	1.52	1.52	1.53	1.53	1.52
C3–C4	1.52	1.52	1.52	1.52	1.52	1.52	1.52	1.52	1.52	1.52
C4–C5	1.53	1.53	1.53	1.52	1.53	1.53	1.53	1.53	1.53	1.53
C5–C6	1.52	1.53	1.53	1.53	1.52	1.52	1.53	1.53	1.51	1.51
C5–O5	1.43	1.44	1.43	1.43	1.42	1.43	1.42	1.43	1.44	1.44
C1–O5	1.42	1.40	1.42	1.40	1.42	1.43	1.2	1.43	1.38	1.37
C1–X	1.39	1.41	1.82	1.87	1.52	1.53	1.44	1.44	1.87	1.86
Bond angles										
C1–O5–C5	113.25	116.03	113.22	116.16	114.33	116.08	108.45	116.01	114.52	116.82
C1–C2–C3	108.97	110.18	109.18	109.98	109.37	110.85	109.03	110.92	109.31	110.49
O5–C1–X	109.59	113.34	109.12	114.25	107.50	113.45	107.87	116.18	106.5	112.16
Dihedral angles										
C2–C1–O5–C5	−62.47	−54.61	−62.00	−56.15	−62.12	−58.09	−65.14	−55.82	−55.21	−54.99
C1–O5–C5–C4	60.60	56.81	62.87	56.28	60.92	58.10	63.41	58.96	56.31	55.90

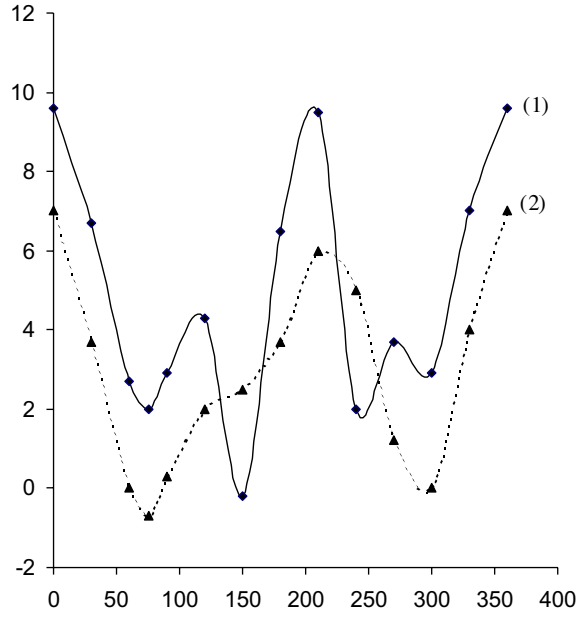

Figure 4. B3LYP/6-311G++** potential energy of rotation about the C5–C6 linkage for methyl β-D-glucopyranoside (solid line, 1) and the ap orientation (dashed line, 2) of the C4 and C6 hydroxyl groups.

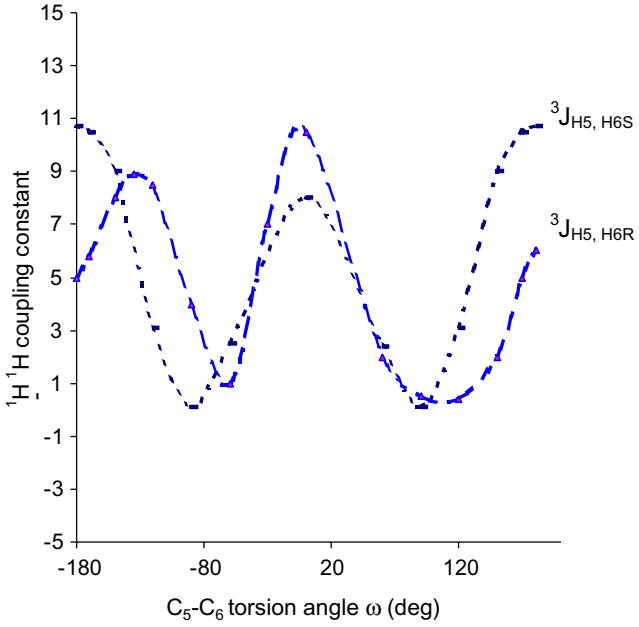

Figure 5. Plots of the dependencies of calculated the $^3J_{H5,H6R}$ and $^3J_{H5,H6S}$ in **7** on the torsion angle, ω.

the O4–H4···O6 hydrogen bond in optimized structures of **1a**. A similar pattern was observed for the galactose derivatives. For example, the conformational profile of **1d** shows two deep minima at $\omega = 220°$ and 330°, which reflect the stabilization by the O6–H6···O4 and O4–H4···O6 hydrogen bonds, respectively.

3.3. Three- and two-bond ^{1}H–^{1}H spin–spin coupling constants

$^3J_{H5,H6R}$, $^3J_{H5,H6S}$, and $^2J_{H6R,H6S}$ (Eqs. 1–3) were computed for compound **7**, using a set of staggered and eclipsed geometries. Figure 5 shows the dependences of $^3J_{H5,H6R}$ and $^3J_{H5,H6S}$ on ω in compound **7**.

$$^3J_{H5,H6R} = 5.06 + 0.45\cos(\omega) - 0.90\cos(2\omega) + 0.80\sin(\omega) + 4.65\sin(2\omega) \quad (\text{rms} = 0.20\ \text{Hz}) \tag{1}$$

$$^3J_{H5,H6S} = 4.86 - 1.22\cos(\omega) + 4.32\cos(2\omega) + 0.04\sin(\omega) + 0.07\sin(2\omega) \quad (\text{rms} = 0.15\ \text{Hz}) \tag{2}$$

Equations for $^3J_{H5,H6R}$ and $^3J_{H5,H6S}$ were also derived by including additional terms to account for a small effect due to rotation about θ, but this refinement did not significantly improve the quality of the parameterization. $^2J_{H6R,H6S}$ is affected by both ω and θ, but the dependence on θ is significantly greater than ω. The latter conclusion is supported by previous studies of Stenutz et al.[14] and Thibaudeau et al.,[20] which showed that the computed $^2J_{H6R,H6S}$ is related to both ω and θ. The additional hypersurface dataset obtained in this work yielded an improved equation (Eq. 3) with a substantially smaller rms error. The following Eq. 3 was obtained for **7** and relates $^2J_{H6R,H6S}$ to ω and θ.

$$^2J_{H6R,H6S} = -10.97 + 0.11\cos(\omega) + 0.59\cos(2\omega) - 0.79\cos(\theta) + 2.00 \times \cos(2\theta) \quad (\text{rms} = 0.41\ \text{Hz}) \tag{3}$$

3.4. One-bond ^{13}C–^{1}H spin–spin coupling constants

The C–H bond length is a key determinant of $^1J_{CH}$ value, with shorter bond (greater s-character) yielding larger couplings.[21] Several structural factors influence C–H bond length: axial versus equatorial bond orientation, vicinal lone-pair effects,[22,23] the 1,3-lone-pair[24] and 1,4-lone-pair effects.[25] The effects of 1,3-interactions with oxygen lone-pairs are observed on $r_{C5,H5}$ and $^1J_{C5,H5}$, therefore the orientation of the vicinal lone-pairs on O5 and the orientation of the C5–H5 bond remain fixed in all structures. A plot of calculated $^1J_{C5,H5}$ versus $r_{C5,H5}$ is linear, Figure 6a indicating that C–H bond length is highly correlated with $^1J_{CH}$ magnitude, with shorter bonds yielding larger coupling constants. The shortest C6–H6 bond and the largest $^1J_{C6,H6}$ values are expected. For the C6–H6 bond that does not experience bond-lengthening due to a vicinal (*anti*) O6 lone-pair interaction and experiences bond-shortening due to a 1,3-interaction with an O5 lone-pair. A plot of calculated $^1J_{C6,H6}$ versus $r_{C6,H6}$, for staggered rotamers is also almost linear (Fig. 6b). The above results relate the $^1J_{C,H}$ to only two torsion angles, ω and θ. Rotation of the C6–O6 bond

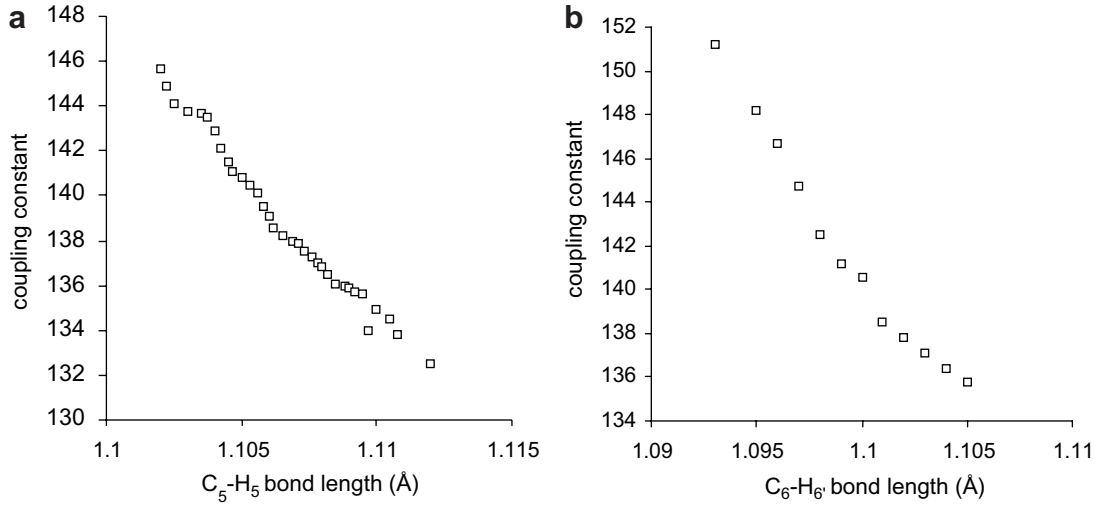

Figure 6. (a) Computed $^{1}J_{C5,H5}$ versus C5–H5 bond length, and (b) computed $^{1}J_{C6,H6}$ versus C6–H6 bond length in **7**. Data were generated from systematic rotations about ω and θ.

modulates the stereoelectronic effect of the O6 lone-pairs on the C6–H6*R* and C6–H6*S* bond lengths, but other effects (1,3-lone-pair interactions with O5 and bond orientation) also influence these bond lengths, so the Karplus equations for compound **7** that relate $^{1}J_{C5,H5}$ and $^{1}J_{C6,H6}$ to ω and θ give relatively large rms errors.

3.5. Two-bond ^{13}C–^{1}H spin–spin coupling constants

The $^{2}J_{CCH}$ values are useful structural constraints in biomolecules such as saccharides and nucleosides and their derivatives.[25] $^{2}J_{C5,H6R}$ and $^{2}J_{C5,H6S}$ are expected to be sensitive to ω. Computed values of these coupling constants are given in Table 3. The dynamic range of $^{2}J_{CCH}$ is $\sim$+5 to −5 Hz ($\Delta \approx 10$ Hz). Two groups of coupling constants are observed at a given ω for each of the three staggered θ rotamers. When OH6 is gauche to both coupled nuclei, a more positive coupling is observed compared to the remaining two staggered rotamers (Fig. 7). The expected C–H and C–C bond elongation may be partly responsible for the shift to more positive couplings. This effect is not observed for $^{2}J_{C6,H5}$, because the C5–O5 torsion is held relatively fixed by the pyranosyl ring and cannot modulate the coupling.

Table 3. Torsion angles, ω and θ (°), and calculated $^{2}J_{CH}$ and $^{3}J_{CH}$ values, (Hz), by the B3LYP/6-311++G** method

ω	θ	$^{2}J_{C5,H6R}$	$^{2}J_{C5,H6S}$	$^{2}J_{C6,H5}$	$^{3}J_{C4,H6R}$	$^{3}J_{C4,H6S}$	C5–C6 rotamer
62	57	−5.2	6.1	−3.51	3.52	2.30	*gt*
57	−48	−3.4	1.92	−3.49	3.10	2.6	
72	192	−5.5	2.6	−4.85	3.50	3.01	
−58	50	2.11	−2.41	2.5	0.15	4.45	*gg*
−70	−72	6.2	−4.85	2.61	3.20	7.2	
−72	171	2.3	−5.21	2.61	5.51	1.50	
176	74	−3.1	−2.21	−3.2	6.52	3.32	*tg*
177	−69	−1.5	−3.91	−3.0	1.50	0.45	
176	176	−4.0	−4.5	−3.7	6.74	3.5	
120	60	−5.5	4.1	−4.8	4.10	0.55	
120	−60	−3.7	0.61	−4.6	4.10	0.37	
120	180	−5.21	−0.4	−5.1	4.10	0.73	
0	60	−1.85	3.51	0.5	6.5	3.80	
0	−60	1.5	−0.5	0.0	6.5	3.50	
0	180	−2.1	−0.5	0.15	6.5	3.60	
120	60	1.2	−4.0	1.0	4.7	7.20	
120	−60	4.50	−6.2	1.42	4.7	7.50	
120	180	0.61	−6.0	1.0	4.7	7.30	

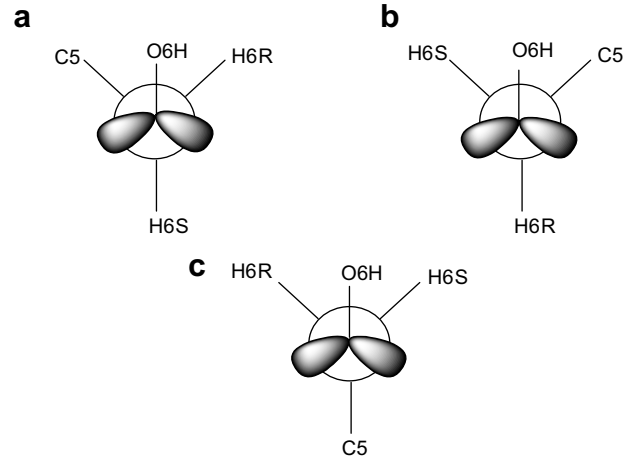

Figure 7. θ rotamers that make a positive contribution to $^{2}J_{C5,H6R}$ (a), $^{2}J_{C5,H6S}$ (b), and $^{2}J_{H6R,H6S}$ (c).

Substitution of an OH group at C4 appears to affect $^{2}J_{C5,H6R}$ and $^{2}J_{C5,H6S}$ values. In this case, the coupling constant is shifted to a more negative value, because of the 1,3-interaction between coupled protons with O4. This interaction may be caused by small changes in C–H bond length induced by an O4 lone-pair effect.[24] In this case, the oxygen lone-pairs are expected to reduce bond lengths slightly, which may lead to the slightly more negative $^{2}J_{CH}$. The effect of C4 hydroxylation on $^{2}J_{C6,H5}$ is also observed only when O4 is in the axial orientation. The coupling is shifted to a more negative value in the three staggered ω rotamers. This observation is consistent with prior reports of 'remote' effects on $^{2}J_{CCH}$ in aldohexopyranosides;[26] oxygen substituents trans to the coupled proton on adjacent carbons shift $^{2}J_{C,H}$ to more negative values. The above discussion reveals a significant effect of C–O bond torsions on $^{2}J_{CCH}$ magnitudes, which were anticipated earlier.[14] To explore this effect further, a full hypersurface was obtained for **7** where ω and θ have been changed in 30° increments from 0° to 360°.

Dependencies of $^{2}J_{C5,H6R}$ and $^{2}J_{C5,H6S}$ on ω and θ were parameterized using the complete dataset of 144 structures from the hypersurface, which yielded Eqs. 4 and 5. Eq. 6 shows the relationship between the $^{2}J_{C6,H5}$ on ω. Attempts to parameterize Eq. 6 by including both dihedral angles did not reduce the rms error significantly.

$$^{2}J_{C5,H6R} = -1.0845 + 0.99\cos(\omega) - 4.15\sin(\omega) - 1.03\cos(2\theta) - 1.61\sin(2\theta) \quad (\text{rms} = 0.55\ \text{Hz}) \quad (4)$$

$$^{2}J_{C5,H6S} = 1.12 + 2.15\cos(\omega) + 3.78\sin(\omega) - 0.95\cos(2\theta) + 1.65\sin(2\theta) \quad (\text{rms} = 0.36\ \text{Hz}) \quad (5)$$

$$^{2}J_{C6,H5} = -1.21 + 1.47\cos(\omega) + 3.57\sin(2\omega) \quad (\text{rms} = 0.35\ \text{Hz}) \quad (6)$$

3.6. Three-bond ^{13}C–H spin–spin coupling constants

The $^{3}J_{C4,H6R}$ and $^{3}J_{C4,H6S}$ have been used previously to make stereochemical signal assignments of H6*R* and H6*S* in ^{1}H NMR spectra of aldohexopyranosyl rings, and in studies of CH_2OH conformation.[27] A Karplus relationship has been reported[28] and was applied recently to interpret $^{3}J_{C4,H6R}$ and $^{3}J_{C4,H6S}$ in aldohexopyranosyl rings.[18] Relationships between $^{3}J_{C4,H6R}$, $^{3}J_{C4,H6S}$, ω and θ were examined for compound **7** using geometrically optimized structures (Table 3). A comparison of calculated $^{3}J_{C4,H6R}$ and $^{3}J_{C4,H6S}$ values reveals that both coupling constants have the same angular dependence.

Karplus dependencies for $^{3}J_{C4,H6R}$ and $^{3}J_{C4,H6S}$ are described by Eqs. 7 and 8. An examination of the applicability of the Karplus equations from theoretical studies of **7** to the analysis of experimental couplings observed in aldohexopyranosyl rings substituted with oxygen on C4 was considered by calculating $^{3}J_{CH}$ in **8** and **9**. The data for **8** and **9** are limited and there is no indication that O4 substitution alters the relationships between $^{3}J_{CH}$ and ω/θ significantly.

$$^{3}J_{C4,H6R} = 3.34 + 0.10\cos(\omega) + 3.17\cos(2\omega) + 0.27\sin(\omega) - 0.55\sin(2\omega) \quad (\text{rms} = 0.35\ \text{Hz}) \quad (7)$$

$$^{3}J_{C4,H6S} = 3.64 + 0.49\cos(\omega) + 0.11\cos(2\omega) - 0.13\sin(\omega) - 3.54\sin(2\omega) \quad (\text{rms} = 0.45\ \text{Hz}) \quad (8)$$

The reliability of experimental angular dependence of $^{3}J_{CH}$ is affected by the following factors: (1) Accuracy of $^{3}J_{CH}$ values measured from NMR data; (2) uncertainty in torsion angles determined from X-ray data; (3) differences in the crystal and solution structures; (4) ensemble averaging of values over local motions in experimental data.[27] The $^{3}J_{C4,H6R}$ and $^{3}J_{C4,H6S}$ calculated using Eqs. 7 and 8 were not predicted accurately using the previous Karplus equations.[18,27] The rms deviation of 1.4 Hz was found between DFT-calculated couplings and those predicted by the previous treatments.

3.7. Three bond ^{13}C–^{1}H coupling constants in 1a, 2a, and 3a

The geometrically optimized **2a** and **3a** were used to calculate $^{3}J_{CXCH}$ values for comparison to coupling behavior reported previously, which were obtained using experimental methods. Because the glycosidic torsion angle, H1–C1–X–C, was constrained by the *exo*-anomeric effect, additional information was needed to explore the torsional dependence of $^{3}J_{CXCH}$ for dihedral angles in the range 60–150°. This 60–150° range of torsion was chosen instead of the −60° to −150° range to

reduce the possibility of steric interactions that adversely affect molecular geometry.

3.7.1. C–O–C–H arrays of bonded atoms. The $^{3}J_{C,O1,C1,H1}$ values were calculated in **1a** and a least-squares fitting of the computed values (Table 4), yield Eq. 9, which is comparable to the Karplus equation proposed previously by Tvaroska et al.[29] obtained from experimental methods, Eq. 10. Curve 1 in Figure 8 is a plot of the computed $^{3}J_{COCH}$ values as a function of dihedral angle φ

$$^{3}J_{COCH} = 6.68\cos^{2}\varphi - 0.89\cos\varphi + 0.11 \quad (\text{rms} = 0.65) \tag{9}$$

$$^{3}J_{COCH} = 5.7\cos^{2}\varphi - 0.6\cos\varphi + 0.5 \tag{10}$$

Agreement between the computed and experimental couplings as a function of dihedral angle φ is fair enough. Factors such as solvation, basis set limitations and small set of geometries may be responsible for the deviations from the experimental data. A plot of the generated $^{3}J_{CH}$ values versus torsion angle, φ, demonstrated that the coupling constant is smallest at the torsion angle of ~90° and is greatest at 180°.

3.7.2. C–S–C–H arrays of bonded atoms. Theoretical relationships among $^{3}J_{C,S,C1,H1}$ and φ were examined for geometrically optimized structures of **2a** in water (Table 4), and the Karplus dependency is described by

Table 4. Calculated vicinal ^{13}C–^{1}H spin couplings (Hz) in **1a**, **2a**, and **3a** in water

Dihedral angle (φ)	Compound		
	1a	**2a**	**3a**
60	3.71	3.29	3.42
80	2.82	2.12	2.34
110	3.68	3.11	3.45
130	4.56	3.96	4.25
150	5.67	5.32	5.59

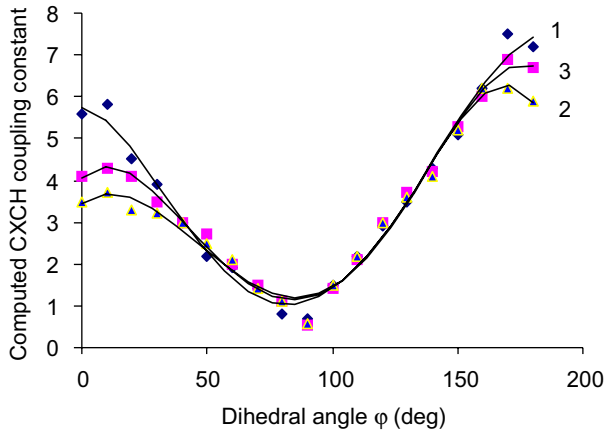

Figure 8. Relationship between $^{3}J_{CH}$ and the C–X–C–H dihedral angle φ for (**1**) X = O, (**2**) X = S, and (**3**) X = C.

Eq. 11. A Karplus-type equation extracted from vicinal carbon proton coupling constants (Eq. 12) has been presented for the C–S–C–H pathway for eight sulfur-containing carbohydrate derivatives.[29] Agreement between the computed and experimental coupling constants as a function of dihedral angle φ is reasonable. Curve 2 in Figure 8 shows the vicinal coupling constants of Eq. 11. The variation of $^{3}J_{CH}$ values with torsion angle in the C–S–C–H segment is smaller than in the C–O–C–H segments.

$$^{3}J_{CSCH} = 5.04\cos^{2}\varphi - 1.35\cos\varphi + 0.55 \quad (\text{rms} = 0.37) \tag{11}$$

$$^{3}J_{CSCH} = 4.44\cos^{2}\varphi - 1.06\cos\varphi + 0.45 \tag{12}$$

3.7.3. C–C–C–H arrays of bonded atoms. The $^{3}J_{C,C,C1,H1}$ computed for **3a** using the optimized structures in water are presented in Table 4 and the resulting Karplus equation is shown by Eq. 13. The results of the calculation are demonstrated by Curve 3 in Figure 8. The same trend was found which the sin terms reflect the small asymmetry around 180°.

$$^{3}J_{CCCH} = 5.78\cos^{2}\varphi - 1.65\cos\varphi + 0.32\sin 2\varphi - 0.031\sin\varphi + 0.57 \quad (\text{rms} = 0.45) \tag{13}$$

3.7.4. Experimental *J*-coupling of α- and β-pyranosides of D-glucose and D-galactose and conformational analysis, qualitative treatment and comparison to theory. The $^{13}C\{^{1}H\}$ and *J*-HMBC spectra with high resolution (error < 0.1) of methyl α- and β-pyranosides of D-glucose and D-galactose provided experimental coupling constants (Table 5). Experimental J_{HH} values in **1a**, **b**, **c**, and **d** (Table 5) are in good agreement with those reported previously[18,20] and $^{1}J_{CH}$ is larger in **1c/d** than in **1a/b**. This enhancement may be attributed to C–H bond orientation (axial vs equatorial) and C4–O4 bond conformation. The equatorial C4–H4 bond in **1c** and **1d** is expected to be shorter than the axial C4–H4 bond in **1a** and **1b**, possibly leading to larger $^{1}J_{C,H}$ in the former. $^{1}J_{C5,H5}$ exhibits a dependence on anomeric configuration, with the α-anomer yielding slightly larger couplings than the β-anomer. This result is consistent with prior studies of oxygen lone prior effects on saccharide C–H bond lengths.[23] The $^{2}J_{C4,H3}$, $^{2}J_{C4,H5}$ and $^{2}J_{C5,H4}$ have negative signs in **1a/b** and positive signs in **1c/d**. These results are consistent with sign predictions based on the projection rule.[30] The $^{3}J_{C4,H2}$ values are slightly larger in **1a** and **1b** than in **1c** and **1d**, possibly due to a small in-plane effect from the equatorial O4.[27] Values of coupling constants were compared to those predicted by Eqs. 1–8 and those calculated from geometrically optimized conformers of the compounds under investigation. The above comparisons reveal that experimental

Table 5. Experimental ^{1}H–^{1}H and ^{13}C–^{1}H spin–spin couplings constants of α- and β-pyranosides of D-glucose and D-galactose in D_2O at 298 K[a]

Coupling	1a	1b	1c	1d
$^{3}J_{H1,H2}$	8.0 (8.0) [8.0]	3.8 (3.8) [3.8]	7.9 (8.0) [7.9]	3.9 (3.9) [4.0]
$^{3}J_{H2,H3}$	9.4 (9.5) [9.4]	9.8 (9.8) [9.8]	9.9 (9.9) [9.9]	10.3 (10.3) [10.3]
$^{3}J_{H3,H4}$	9.2 (9.2) [9.2]	9.1 (9.2) [9.1]	3.5 (3.5) [3.4]	3.5 (3.4) [3.4]
$^{3}J_{H4,H5}$	9.7 (10.0) [9.7]	10.0 (10.0) [10.1]	1.1 (1.1) [1.1]	1.2 (1.2) [1.0]
$^{3}J_{H5,H6R}$	6.0 (6.2) [6.0]	5.4 (5.6) [5.5]	7.9 (7.9) [7.9]	8.2 (8.2) [7.2]
$^{3}J_{H5,H6S}$	2.3 (2.3) [2.0]	2.3 (2.3) [2.3]	4.4 (4.4) [4.4]	4.2 (4.2) [5.2]
$^{2}J_{H6R,H6S}$	−12.3 (−12.4) [−12.3]	−12.3 (−12.4) [−12.3]	−11.8 (−11.8) [−11.7]	−11.7 (−11.7) [−11.7]
$^{1}J_{C4,H4}$	144.8	144.4	146.2	146.5
$^{1}J_{C5,H5}$	141.7	144.3	140.8	143.5
$^{1}J_{C6,H6R}$	143.2	143.2	145.5	145.1
$^{1}J_{C6,H6S}$	144.5	144.2	142.9	142.5
$^{2}J_{C4,H3}$	−4.7	−4.7	1.6	1.6
$^{2}J_{C4,H5}$	−2.8	−2.9	3.3	3.0
$^{2}J_{C5,H4}$	−4.0	−3.8	1.0	1.1
$^{2}J_{C5,H6R}$	−2.5	−1.9	−5.0	5.1
$^{2}J_{C5,H6S}$	−1.1	−1.4	0.4	1.0
$^{2}J_{C6,H5}$	−2.3	−1.4	−5.5	−5.2
$^{3}J_{C4,H2}$	1.1	1.0	0.7	0.9
$^{3}J_{C4,H6R}$	1.0	1.1	1.9	1.0
$^{3}J_{C4,H6S}$	2.4	2.9	4.0	3.7
$^{3}J_{C5,H3}$	1.1	1.0	—	0.5
$^{3}J_{C6,H4}$	3.6	3.6	1.0	1.0

[a] Data in parentheses were taken from Thibaudeau et al.[20] and data in brackets were taken from Tvaroska et al.[18]

and calculated *J*-coupling values differ by ∼1 Hz and produced equations can be applied quantitatively in conformational analysis of glucose and galactose derivatives.

4. Conclusions

The present study focused on free CH_2OH groups and bonds involving the anomeric center in 24 aldohexopyranosides to establish new *J*-coupling structure correlations. The application of these correlations has practical benefits, for example, in oligosaccharides where intramolecular H-bonding may influence ω or θ. New structural constraints to assess CH_2OH group conformation in saccharides based on multiple, redundant *J*-couplings have been described in this report. Using theoretical and experimental methods, Karplus equations were developed to correlate the magnitudes and signs of eight scalar couplings describing CH_2OH conformation. Interestingly, some of these couplings display dependence not only on ω but also on θ. These dependencies serve as indirect investigations of C6–O6 bond conformation in solution and do not depend on direct observation of the exchangeable hydroxyl proton. Therefore, the application of these equations allows the estimation of correlated conformations about ω and θ. This report also generates new theoretical treatments of $^{3}J_{CXCH}$ of carbohydrates that make the interpretation of oligosaccharide conformational analysis feasible. In addition our investigations increase the present database of $^{3}J_{COCH}$, $^{3}J_{CSCH}$, and $^{3}J_{CCCH}$ in O-glycosidic, thioglycosidic, and C-glycosidic linkages and permit a more comprehensive testing of their utility as conformational constraints in these systems. Therefore, this theoretical study generalized a quantitative tool to calculate J_{HH} and J_{CH} values in saccharides, which involves comparisons of calculated and experimental coupling constants in conformationally constrained system. The present findings are a significant contribution not only for studies of oligosaccharides but also for related studies on oligonucleotides.

Acknowledgments

The authors thank Professor Hiroshi Sugiyama from Tohoku University for his valuable advice and suggestions. We are grateful to the Ministry of Science, Research and Technology for financial support. Also, we have thanks to IDB for purchasing the NMR instrument.

References

1. Benedict, H.; Shenderovich, I. G.; Malkina, O. L.; Malkin, V. G.; Denisov, G. S.; Golubev, N. S.; Limbach, H. H. *J. Am. Chem. Soc.* **2000**, *122*, 1979–1988.
2. Cornilescu, G.; Bax, A.; Case, D. A. *J. Am. Chem. Soc.* **2000**, *122*, 2168–2171.
3. Malkina, O. L.; Hricovini, M.; Bizik, F.; Malkin, V. G. *J. Phys. Chem. A* **2001**, *105*, 9188–9195.
4. Homans, S. W. *Prog. NMR Spectrosc.* **1990**, *22*, 55–81.
5. Yan, Z. Y.; Bush, C. *Biopolymers* **1990**, *29*, 799–811.

6. Meissner, A.; Soerensen, O. W. *Magn. Reson. Chem.* **2001**, *39*, 45–49.
7. Frisch, M. J.; Trucks, G. W.; Schlegel, H. B.; Scuseria, G. E.; Robb, M. A.; Cheeseman, J. R.; Zakrzewski, V. G; Montgomery, J. A.; Stratmann, R. E.; Burant, J. C.; Dapprich, S.; Millam, J. M.; Daniels, A. D.; Kudin, K. N.; Strain, M. C.; Farkas, O.; Tomasi, J.; Barone, V.; Cossi, M.; Cammi, R.; Mennucci, B.; Pomelli, C.; Adamo, C.; Clifford, S.; Ochterski, J.; Petersson, G. A.; Ayala, P.Y.; Cui, Q.; Morokuma, K.; Malick, D. K.;. Rabuck, A. D.; Raghavachari, K.; Foresman, J. B.; Cioslowski, J.; Ortiz, J. V.; Stefanov, B. B.; Liu, G.; Liashenko, A.; Piskorz, P.; Komaromi, I.; Gomperts, R.; Martin, R. L.; Fox, D. J.; Keith, T., Al-Laham, M. A.; Peng, C. Y.; Nanayakkara, A.; Ghonzalez, C. V.; Challacombe, M.; Gill, P. M. W.; Johnson, B. G.; Chen, W.; Wong, M.; Andres, J. L.; Head-Gordon, M.; Replogle E. S.; Pople, J. A. GAUSSIAN *2003 (Revision-B)*; Gaussian: Pittsburgh, PA, 2003.
8. Beck, A. D. *J. Chem. Phys.* **1993**, *98*, 5648–5652.
9. Parr, R. G.; Yang, W. *Density-Functional Theory of Atoms and Molecules*; Oxford University: New York, 1989.
10. Bose, B.; Zhao, S.; Stenutz, R.; Clorn, F.; Bondo, P.; Bondo, G.; Hertz, B.; Carmichael, I.; Seianni, A. S. *J. Am. Chem. Soc.* **1998**, *120*, 11158–11173.
11. Li, J. H.; Ma, B.; Allinger, N. L. *J. Comput. Chem.* **1999**, *20*, 1593–1603.
12. Cloran, F.; Carmichael, I.; Serianni, A. S. *J. Phys. Chem. A* **1999**, *103*, 3783–3795.
13. Kowalewski, J.; Laaksonen, A.; Root, B.; Siegbahn, P. *J. Chem. Phys.* **1979**, *71*, 2896–2902.
14. Stenutz, R.; Carmichael, I.; Widmalm, G.; Serianni, A. S. *J. Org. Chem.* **2002**, *67*, 949–958.
15. Lemieux, R. U. *Can. J. Chem.* **1987**, *65*, 213–223.
16. Ivarsson, I.; Sandström, C.; Sandström, A.; Kenne, L. *J. Chem. Soc., Perkin Trans. 2* **2000**, 2147–2152.
17. Tomasi, J.; Barone, V.; Cossi, M. *J. Comp. Chem.* **1998**, *19*, 404–409.
18. Tvaroska, I.; Taravel, F. R.; Utille, J. P.; Carver, J. P. *Carbohydr. Res.* **2002**, *337*, 353–367.
19. Tvaroska, I.; Carver, J. P. *J. Phys. Chem. B* **1997**, *101*, 2992–2999.
20. Thibaudeau, C.; Stenutz, R.; Hertz, B.; Klepach, T.; Zhao, S.; Wu, Q.; Carmichael, I.; Serianni, A. S. *J. Am. Chem. Soc.* **2004**, *126*, 15668–15685.
21. Serianni, A. S.; Wu, J.; Carmichael, I. *J. Am. Chem. Soc.* **1995**, *117*, 8645–8650.
22. Podlasek, C. A.; Stripe, W. A.; Carmichael, I.; Shang, M.; Basu, B.; Serjanni, A. S. *J. Am. Chem. Soc.* **1996**, *118*, 1413–1425.
23. Kennedy, J.; Wu, J.; Drew, K.; Carmichael, I.; Serjanni, A. S. *J. Am. Chem. Soc.* **1997**, *119*, 8933–8945.
24. Cloran, F.; Zhu, Y.; Osborn, J.; Carmichael, I.; Serianni, A. S. *J. Am. Chem. Soc.* **2000**, *122*, 6435–6448.
25. Stenutz, R.; Carmichael, I.; Widmalm, G.; Serianni, A. S. *J. Org. Chem.* **2002**, *67*, 949–958.
26. Podlasek, C. A.; Wu, J.; Stripe, W. A.; Bondo, P.; Serianni, A. S. *J. Am. Chem. Soc.* **1995**, *117*, 8635–8644.
27. Tvaroska, I.; Gajdos, J. *Carbohydr. Res.* **1995**, *271*, 151–162.
28. Tvaroska, I.; Hricovini, H.; Petrakova, E. *Carbohydr. Res.* **1989**, *189*, 359–362.
29. Tvaroska, I.; Mazeau, K.; Blanc-muesser, M.; Lavaitte, S.; Driguez, H.; Taravel, F. R. *Carbohydr. Res.* **1992**, *229*, 225–231.
30. Bock, K.; Pedersen, C. *Acta Chem. Scand., Ser. B.* **1977**, *31*, 354–358.